

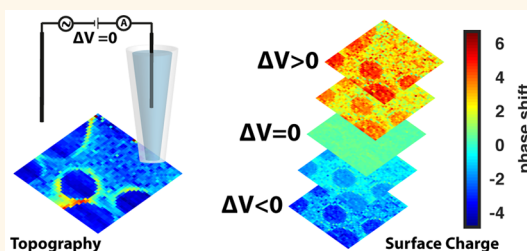
Simultaneous Nanoscale Surface Charge and Topographical Mapping

David Perry,^{†,‡,§} Rehab Al Botros,^{†,§} Dmitry Momotenko,^{†,§} Sophie L. Kinnear,[†] and Patrick R. Unwin^{*,†}

[†]Department of Chemistry and [‡]MOAC Doctoral Training Centre, University of Warwick, Coventry CV4 7AL, United Kingdom. [§]These authors contributed equally.

ABSTRACT Nanopipettes are playing an increasingly prominent role in nanoscience, for sizing, sequencing, delivery, detection, and mapping interfacial properties. Herein, the question of how to best resolve topography and surface charge effects when using a nanopipette as a probe for mapping in scanning ion conductance microscopy (SICM) is addressed. It is shown that, when a bias modulated (BM) SICM scheme is used, it is possible to map the topography faithfully, while also allowing surface charge to be estimated. This is achieved by applying zero net bias between the electrode in the SICM tip and the one in bulk

solution for topographical mapping, with just a small harmonic perturbation of the potential to create an AC current for tip positioning. Then, a net bias is applied, whereupon the ion conductance current becomes sensitive to surface charge. Practically this is optimally implemented in a hopping-cyclic voltammetry mode where the probe is approached at zero net bias at a series of pixels across the surface to reach a defined separation, and then a triangular potential waveform is applied and the current response is recorded. Underpinned with theoretical analysis, including finite element modeling of the DC and AC components of the ionic current flowing through the nanopipette tip, the powerful capabilities of this approach are demonstrated with the probing of interfacial acid–base equilibria and high resolution imaging of surface charge heterogeneities, simultaneously with topography, on modified substrates.



KEYWORDS: nanopipette · surface charge · scanning ion conductance microscopy · SICM · double layer · impedance · finite element method modeling

Surface charge density plays an important role in interfacial processes and properties, and being able to probe surface charge in a simple, robust manner could find great application in mineralogy,^{1–3} colloidal science,^{4–7} materials science, including the study of electrode surfaces,⁸ and in living systems^{4,9–16} where surface charge is known to play a key role. While zeta potential measurements^{17,18} and potentiometric titrations^{19–21} give important information on the charge of colloids in solutions, the charge on extended surfaces is more difficult to probe, with relatively few techniques available. Since surfaces are often characterized by both heterogeneous charge distributions and topographical features, scanning probe microscopes (SPMs), such as force microscopy (FM)^{22–26} and scanning ion conductance microscopy (SICM),^{27–32} are potentially attractive as a means of probing local surface charge. At the same time, because the response of these techniques depends on both topography and surface charge (and other properties), there is a wider

consideration about the operation of these SPMs, and the extent to which these different effects are convoluted in the response.

This paper describes how SICM can be used to (i) measure topography largely free from surface charge effects and (ii) how the corresponding charge on the surface can be probed semiquantitatively. SICM uses a positionable nanopipette to examine electrolyte–substrate interfaces without requiring a direct mechanical contact with the substrate itself, making it a powerful approach for the investigation of soft (biological) samples.^{27,32,33} Traditionally in SICM, a bias is applied between a quasi-reference counter electrode (QRCE) in the nanopipette tip and a second QRCE in bulk solution to generate a direct ionic current (DC). Away from the surface, the total resistance of this conductometric cell is dominated by the contribution from the narrow tip opening. As the tip approaches the surface to within a tip diameter, the resistance contribution from the tip-to-substrate gap increases and causes the value of ionic

* Address correspondence to p.r.unwin@warwick.ac.uk.

Received for review April 8, 2015 and accepted July 1, 2015.

Published online July 01, 2015
10.1021/acs.nano.5b02095

© 2015 American Chemical Society

current to drop.²⁷ This provides a means of monitoring the surface topography, using various schemes such as distance modulation (DM)^{27,28,30,34} and the hopping (backstep) mode^{32,35,36} in which a specific tip current value is used to maintain a fixed tip–surface separation during scanning. In DM-SICM, a harmonic oscillation to the vertical (*z* axis) position is applied and an alternating current signal (AC) is induced, the amplitude of which can be used for positionable feedback.^{27,28,30,34} Typically, under high electrolyte conditions any double layer formed at charged interfaces is considered to be compressed to an undetectable level,³⁷ and so it has been argued that surface charge does not convolute recorded signals, enabling topography to be faithfully reproduced²⁹ within the framework of traditional SICM experiments.

For lower electrolyte conditions (most prominently below 10 mM), the diffuse double layer (DDL) at charged interfaces expands further into solution, with a Debye length of a few nanometers in aqueous solution, and even more in media with lower dielectric constants and/or lower ionic strength.³⁸ This effect leads to ion current rectification phenomena at nanopipette tips in bulk solution^{39–41} as well as surface induced rectification,^{42,43} once a nanopipette approaches toward a charged surface. Indeed, near a surface, there is a polarity-dependent current enhancement or diminution, due to the double layer at the surface modulating the transport of ions traveling through the nanopipette opening,^{42,44} in contrast to the expectations of the operation of conventional SICM.²⁷ This phenomenon has recently been explored and used to map surface charge heterogeneities using a classical DM-SICM setup.⁴⁴ However, there are a number of issues with this technique. The mechanical oscillation of the tip in DM-SICM limits the range of working distances achievable with the nanopipette and consequently the sensitivity and resolution. Furthermore, the high-speed motion of the probe and fluid exerts mechanical forces on the sample, which may influence its response, for example, when living cells are studied. The requirement of a large bias between the two QRCEs has also been suggested to lead to fluidic instabilities which impact on the surface.⁴³ Finally, for smaller probes, it becomes especially difficult to separate topography and surface charge.⁴⁴

We have recently proposed an alternative approach for positionable feedback control of nanopipettes in SICM, whereby the tip-to-substrate separation is controlled through the application of an oscillating bias between the two QRCEs to generate an AC signal.⁴⁵ It has been demonstrated that at high electrolyte concentrations, bias modulated (BM)-SICM provides a stable feedback for tracking surface topography with oscillation around 0 V between the two QRCEs, at a range of frequencies using either the AC amplitude or AC phase signals. In this paper, we reveal the

capabilities of BM-SICM for accurate tracing of the surface topography at charged substrates, at low electrolyte concentrations, by minimizing (virtually eliminating) polarity dependent effects of surface charge in the conductometric response. Moreover, we further highlight the possibility of probing and mapping unevenly distributed charge at interfaces by sensing of the local ionic environment within a double layer. This is achieved through the use of a *hopping approach* and *CV measurement* at each pixel in an image, with certain biases between the two QRCEs shown to highlight surface charge in a sensitive manner, while, for others, the current response is insensitive to the surface charge, thus revealing only the topography with high precision. With the aid of finite element method (FEM) modeling, we verify the experimental observations and demonstrate the sensitivity of the AC voltammetric response to the double layer and charge at target surfaces. As well as independent and simultaneous topographical and surface charge imaging, this work provides a robust platform for future local nanoscale impedance experiments.

RESULTS AND DISCUSSION

Bias Modulated-SICM as an Ion-Sensing Probe of Double Layers. An uncompensated surface charge in electrolyte solutions leads to the formation of a diffuse double layer, consisting of co- and counterions that balance the charge. The approach herein is to probe the ionic atmosphere of the double layer electrochemically (conductometrically) with a nanopipette and derive surface charge information. At low electrolyte concentrations, glass (or quartz) nanopipettes with small tip openings exhibit perm-selectivity^{39,40} toward counterions of the DDL that have enhanced concentration near the charged nanopipette walls. In combination with asymmetric mass-transport rates inside and outside nanopipettes (taking into account the geometrical configuration of the probe), the absolute value of ionic current driven through the opening becomes polarity-dependent and this diode-like behavior is known as ion current rectification (ICR).^{39–41,46,47}

When a nanopipette approaches a charged surface, the rectifying characteristics of the probe can be modified due to the presence of the DDL at the surface.^{42,44} As a result, the surface-induced rectification contributes significantly to the overall mass-transport properties of the nanopipette and, in principle, this effect can be employed for probing and mapping surface charge.⁴⁴ However, as mentioned in the introduction, the DC or AC components of ionic current are also distance-dependent, and this presents a conundrum as to how to separate charge and distance effects in the conventional DM-SICM scheme. Essentially, in DM-SICM the ionic current driven through the nanopipette cannot necessarily be reliably employed for either task—probing the surface charge or tracking the

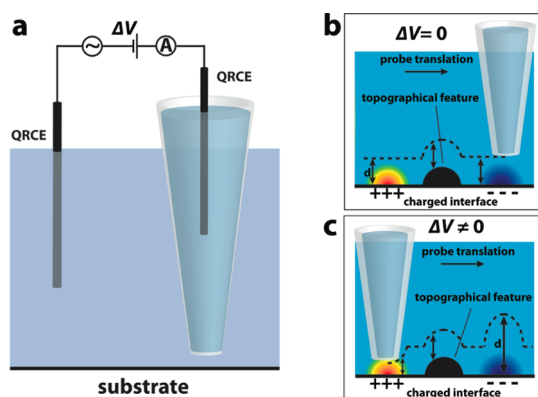


Figure 1. Concept of simultaneous topographical and charge mapping with a positionable nanopipette. (a) Schematic representation of the bias-modulation SICM (BM-SICM) setup. Graphical representation (not to scale) demonstrating deconvoluted (b) and hypothetically convoluted (c) scanning over a sample containing topographical (shown in black) and charge features (double layer over positively and negatively charged areas are shown in rainbow and blue gradients, respectively). The possible probe trajectory for a fixed set point (target distance, d) is shown as a dashed line.

topography.⁴⁴ For surfaces with large topographical features and relatively low surface charge densities, the implications of this may not be noticeable,⁴⁴ but as the resolution of the technique is advanced with smaller nanopipettes being utilized and smaller topographical features being probed,^{36,48} the resulting effects of surface charge heterogeneities on the DM-SICM feedback may become much more apparent.

Herein, we present an elegant way to resolve both surface topography and charge by using BM-SICM (Figure 1a). In a BM-SICM configuration, a small harmonic oscillation of potential is applied to induce an AC ionic current component, which can be used for vertical probe positioning even in the absence of mean bias applied between two QRCEs.⁴⁵ Additionally, by applying an additional bias, ΔV , we show herein that one can control the extent to which the SICM current response is sensitive (or not) to surface charge. In essence for $\Delta V = 0$, the BM-SICM response faithfully maps topography (Figure 1b), due to minimal surface induced rectification about 0 V, while for $\Delta V \neq 0$, the SICM response becomes surface charge sensitive. Note that by maintaining $\Delta V = 0$ on approach for *topographical imaging* in this work, the scenario of traditional SICM experiments is avoided where, based on recent work,^{42,44} an applied bias upon approach to heterogeneously charged substrates may result in a nonconstant working distance and hence distorted topography (Figure 1c).

To demonstrate the efficacy of BM-SICM for probe positioning near a surface, independent of surface functionality, a series of nanopipette approaches toward positively (3-aminopropyl triethoxysilane, APTES) and negatively (glass) charged substrates were carried out at different nanopipette biases, applied to the

probe. Here the distance, d , was defined with respect to the distance of closest approach, *ca.* 25 nm or less. For simulations, d is the absolute tip–substrate distance. These approach curves, and all experimental and simulation studies herein, were performed using an oscillation frequency of 270 Hz. This frequency was selected based on our recent work⁴⁵ and impedance studies performed herein (see Supporting Information, section SI-2) that highlight a frequency domain where the AC phase is most sensitive to changes in both system capacitance and resistance. This region is where the slope of the Bode plot of AC phase against frequency is greatest, which can be seen to exist between 100 Hz and 1 kHz, for the experimental conditions of the experiments herein (Supporting Information, Figure S2). Below this frequency range, the phase is zero, as the current solely passes through the resistive component of the system. Above this frequency range, the current is dominated by the capacitive component of the system.

As expected, based on recent DM-SICM studies,^{42,44} at close probe–substrate separations in BM-SICM surface-induced rectification influences the mass-transport of ions, leading to surface-enhanced or diminished ion current values, compared to the bulk to which currents are normalized (Figure 2a,b), depending on the substrate charge and the SICM bias polarity. The AC phase shift (which we define throughout as the distance-dependent phase with respect to that with the nanopipette in bulk) is particularly sensitive to the presence of surface charge at the substrate when $\Delta V \neq 0$ (see Figure 2c,d), an aspect we explore further below with FEM simulations. The AC amplitude also exhibits a dependence on the substrate surface charge, albeit weaker, seen to be enhanced under the same conditions as the DC enhancement and diminished with decreasing DC values (see Supporting Information, SI-3 for AC amplitude approach curves recorded simultaneously with the data in Figure 2). Interestingly, although these effects are manifested at low ionic strength, for reasons outlined in the introduction, they can be seen at relatively high ionic strength, up to 0.1 M, even though the magnitude of the effect decreases with increasing concentrations (see Supporting Information SI-4 for data). These data have important implications for how topographical SICM experiments are designed (to avoid charge effects), but could also be exploited to allow for the probing of the double layer at biological samples *in vivo*, which require a physiological environment (relatively high ionic strength) for viability. Note that the data are especially significant as we have used a relatively large SICM tip for these studies, and the effects seen at high ionic strength would be magnified with smaller tip sizes deployed at closer sample distances.

A major observation in Figure 2 is that with no mean bias ($\Delta V = 0$, with just a small amplitude oscillation of

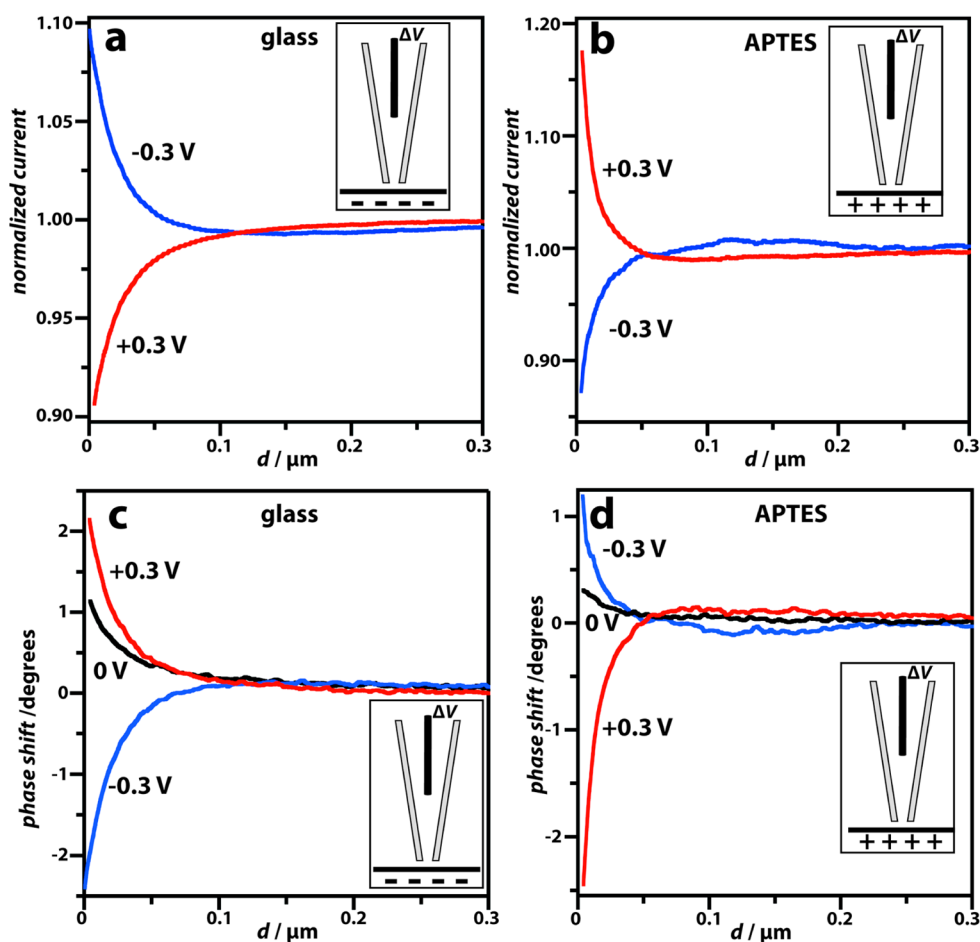


Figure 2. Experimental approach curves depicting normalized DC ion current (a and b); and phase shift (c and d) behavior as a function of the probe-to-substrate distance, d , recorded with ≈ 75 nm radius nanopipette over negatively charged glass and positively charged APTES substrates at 0.3 V (red lines), -0.3 V (blue lines), and 0 V (black lines) bias offset (ΔV) values. Schematic illustrations, as insets, depict the nanopipette approaching variously charged substrates for the corresponding plots. The DC ionic currents are normalized to the respective values at solution bulk, while the phase shifts are reported with respect to the corresponding bulk values. The DC data at 0 V are not presented, as there is no significant ion flow.

the bias between the QRCEs) the phase shift is intrinsically a *distance-dependent quantity* and is relatively *insensitive to surface charge*. The phase of the AC current (with respect to the bulk response) shifts slightly positive over both the negatively charged glass substrate and positively charged APTES functionalized substrate (Figure 2c,d). To account for these AC effects, and to assess BM-SICM for topographical and charge mapping, finite element simulations were used to study the AC and DC SICM response toward a harmonic perturbation of the electric potential.

Theory and Simulations. The simulation of the harmonic perturbation of the DDL due to an applied alternating potential is a complicated task, especially in a nanopore or nanopipette configuration, and a typical treatment of this problem is performed in terms of equivalent electrical circuits.^{45,49} Here, we adopt a more general approach by studying the ionic transport and ion distributions, from which we can derive the resulting impedance response, using finite element method modeling.

Ions are considered as point charges, while ionic transport is assumed to follow the classical Nernst–Planck relationship, where the flux, J_i , of species, i is given as

$$J_i = -D_i \nabla c_i - z_i \frac{F}{RT} D_i c_i \nabla \phi \quad (1)$$

while the Poisson equation describes the electrical potential ϕ :

$$\nabla^2 \phi = -\frac{F}{\epsilon \epsilon_0} \sum_i z_i c_i \quad (2)$$

Here, c_i denotes the species concentration, while D_i , z_i , F , R , T , ϵ , and ϵ_0 specify constants: system diffusion coefficient of i , its charge number, the Faraday constant, gas constant, temperature, relative permittivity, and vacuum permittivity, respectively.

Throughout this work, a surface charge density on the nanopipette tip was assumed to be -1.125 mC m^{-2} (140 nm^2 per ionized site), consistent with previously reported simulations.^{40–42,50,51} However, the actual

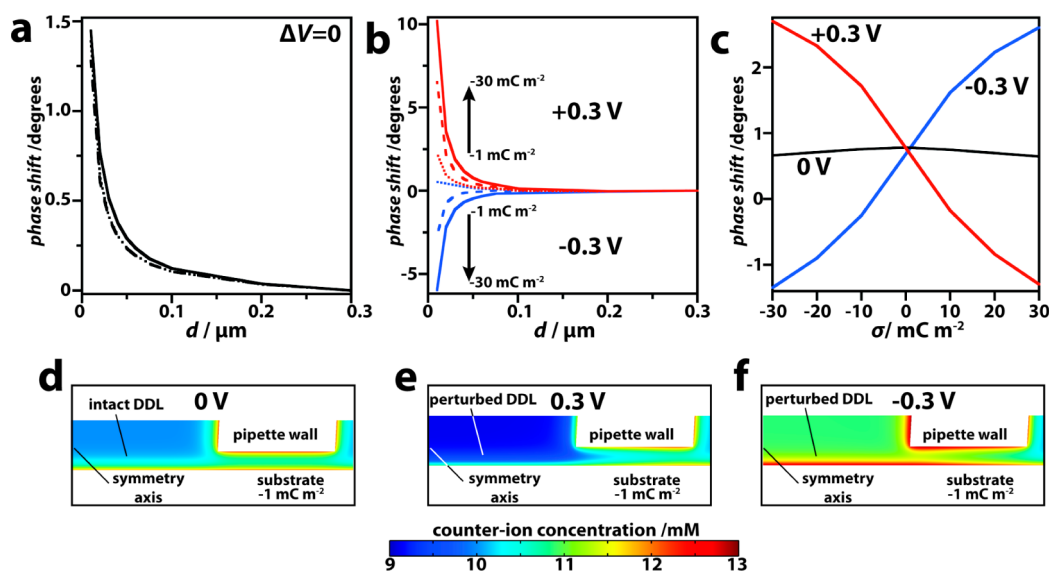


Figure 3. (a) Simulated BM-SICM approach curves in the absence of mean bias offset ($\Delta V = 0$) at 270 Hz, 10 mV rms amplitude bias modulation over a substrate carrying surface charge densities, σ , of 0 (solid), -30 (dotted), and $+30$ (dashed) mC m^{-2} . (b) A series of simulated approaches toward a negatively charged surface (σ values -30 (solid), -10 (dashed) and -1 (dotted) mC m^{-2} with the arrows indicating an increase of the absolute magnitude of the surface charge density) at bias values of $+0.3$ V (red lines) and -0.3 V (blue lines). (c) Theoretically predicted values of the phase shift of the ion current passing through a 75 nm radius nanopipette positioned at 25 nm from a charged surface at 0, -0.3 , and $+0.3$ V bias (black, blue, and red lines, respectively). (d–f) Calculated steady-state concentration profiles of DDL counterion, for a DC bias only, near a nanopipette tip positioned 10 nm above a charged interface ($\sigma = -1 \text{ mC m}^{-2}$) at (d) 0 V, (e) $+0.3$ V, and (f) -0.3 V bias. Note that only half of the symmetric nanopipette cross section is shown.

density of ionizable sites strongly depends on the nature of the material and could vary within the range of microcoulombs to a few hundreds of millicoulombs per squared meter of a surface.^{42,52–55}

The system of differential eqs 1 and 2 was solved with appropriate boundary conditions (see section SI-1 and Table S1, Supporting Information), for a particular ΔV and assuming flux conservation in a first step (eq 3)

$$\nabla J_i = 0 \quad (3)$$

Then, for AC analysis, a harmonic bias modulation was applied between the two QRCEs in the form of a linearized perturbation in the frequency domain

$$\nabla J_i = j\omega c_i \quad (4)$$

where j is the imaginary unit and ω is the angular frequency (full details of the FEM simulations are given in section SI-1, Supporting Information).

This approach provides a powerful framework to study the impedance response both in bulk (see for example Figure S2, Supporting Information SI-2) and with a nanopipette positioned at different separations from a charged or uncharged substrate. As highlighted earlier in Figure 2, the experimental phase shift with zero net bias, $\Delta V = 0$, as a function of distance appeared relatively insensitive to the surface charge, while for an applied bias ($\Delta V \neq 0$), there was a surface-charge dependent phase shift.

Figure 3a shows simulated approach curves toward substrates with applied surface charge of $\pm 30 \text{ mC m}^{-2}$ (5 nm^2 per ionized site) and 0 mC m^{-2} . It can be seen

that the model predicts the phase shift of the induced harmonic ion current to be almost independent of surface charge when there is no DC bias offset between the QRCEs, similar to the experimental observations in Figure 2c,d. This effect has a very important consequence for careful (and accurate) probe positioning over a sample surface, as the phase shift value is an intrinsically sensitive quantity that evidently depends predominantly on the tip-to-substrate distance when $\Delta V = 0$. Under these conditions, Figure 3a (and Figure 2c,d) make it clear that with $\Delta V = 0$, the phase shift can be used as a set point for determining topography and being able to position the probe at close tip-to-substrate separations, which is important for enhancing the resolution of SICM.^{56,57}

In a similar way to the experimental approaches at nonzero bias (Figure 2), the model predicts a dramatic change of the phase-distance behavior for $\Delta V \neq 0$. Figure 3b depicts theoretically predicted approach curves that demonstrate the sensitivity of the AC phase to surface charge. The AC phase shift can be seen to be negative under conditions when an enhanced ionic current is observed, that is, when negative ΔV is applied to the tip QRCE with a negatively charged substrate. In this case the system resistance, upon approaching the substrate, decreases and so more current flows through the resistive component of the system, resulting in the phase tending more toward 0 degrees, thus explaining the negative phase shift from the bulk value, which is between 0 and 90° (Supporting Information SI-2, Figure S2). It can further be seen that

the magnitude of the effect scales with the surface charge density, as would be expected. As the polarity of the bias is reversed, so that the nanopipette QRCE is positive, the negatively charged substrate now induces a diminution of the ionic current and a positive shift in the phase is observed. In this case, the system resistance increases as the tip approaches, so more current flows through the capacitive component of the system and the phase tends to increase toward 90° . Thus, a positive phase shift from that with the nanopipette in bulk is observed. The simulated DC signal mirrors this behavior (Supporting Information SI-5, Figure S5) with the DC current increasing compared to the bulk at close tip–substrate distances (negatively charged substrate) with positive bias on the nanopipette QRCE, but decreasing at negative bias.

From these data it is clear that even a relatively small surface charge (down to 1 mC m^{-2} , equivalent to 160 nm^2 per ionized site) leads to strong variation of the phase shift with bias, that is particularly noticeable when the probe is brought in close proximity to a substrate (especially, at distances below one tip radius, $d < r_{\text{tip}}$). This effect, revealed with an applied bias, can therefore be employed for mapping surface charge with the nanopipette held at a constant distance above the specimen during scanning, as considered below.

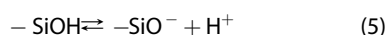
Figure 3c shows the phase shift with a 75 nm radius nanopipette positioned 25 nm above a charged substrate, as a function of surface charge density for 3 biases, $\Delta V = +0.3, 0,$ and -0.3 V . The plots clearly illustrate the sensitivity of the technique, at a constant probe-to-substrate distance, to distinguish between values of surface charge. Importantly, at 0 V bias, a wide range of surface charges have little influence on the phase, making this condition ideal for detecting surface topography, as discussed above. The sensitivity (magnitude) of the phase to a particular surface charge is similar at both positive and negative bias polarities, although the technique offers slightly higher sensitivity in cases when surface-induced rectification acts to enhance the ionic current (e.g., at negative tip bias over a positively charged surface or at positive tip bias over a negatively charged surface).

The reasons for the striking effect of bias on the phase response (Figure 3) and DC current response of BM-SICM (Figure 2) with charged surfaces becomes apparent from the distribution of electrical potential and ion concentrations near the tip opening (when held in the proximity of a surface). With a 0 V bias offset, there is almost no perturbation of the DDL at the substrate, which remains intact. The application of bias, however, is known to lead to ICR inside the nanopipette itself^{39–41} (when it is freely suspended in bulk) and a surface-induced rectification.⁴⁴ This causes a drastic change in the nanopipette conductance state depending on bias polarity and surface charge due to a significant change of ionic conductivities (and therefore,

the overall resistance) within and near the tip opening (see Figure 3, panels e and f for ΔV values of $+0.3$ and -0.3 V , respectively). In turn, the AC ion current components, particularly the phase shift, which are highly sensitive to the overall resistance, as explained above, also demonstrate a strong dependence to the nature of the charged interface.

Probing Acid–Base Equilibria at Interfaces. To illustrate the capabilities of BM-SICM for sensing variations of surface charge, a series of approaches toward glass substrates were carried out as a function of bulk pH (surface titration experiments).

The electrostatic charge on glass and silica surfaces is typically attributed to the presence of silanol groups (SiOH) due to the following acid–base equilibrium:



The dissociation process, however, is rather complicated and depends on the particular type of silica and any surface treatment. In a first approximation, the degree of dissociation depends on the inherent properties of the glass–electrolyte interface (given by the intrinsic dissociation constant, K_{int}) as well as the electrostatic potential on the surface, ψ_0 .⁵⁸

$$\frac{[\text{H}^+]\Gamma_{\text{SiO}^-}}{\Gamma_{\text{SiOH}}} = K_{\text{int}} \exp\left[\frac{F\psi_0}{RT}\right] \quad (6)$$

A broad range of silica interfaces show a $\text{p}K_{\text{int}}$ in the range $7-7.5$.^{52,54} and the surface charge density, σ , can be estimated, using eq 6 along with mass-conservation, which defines the surface concentrations of protonated and deprotonated sites (Γ_{SiOH} and Γ_{SiO^-} , respectively)

$$\sigma = -e\Gamma_{\text{SiO}^-} = -e\Gamma_{\text{total}} \frac{K_{\text{int}} 10^{\text{pH}} \exp\left[\frac{F\psi_0}{RT}\right]}{1 + K_{\text{int}} 10^{\text{pH}} \exp\left[\frac{F\psi_0}{RT}\right]} \quad (7)$$

where Γ_{total} represents the total number of silanol groups per unit area and e is the elementary charge. The surface potential can be calculated from the Grahame equation (for monovalent electrolyte ions present at c_0 bulk concentration):⁵⁸

$$\sigma = (8RT\epsilon\epsilon_0 c_0)^{1/2} \sinh\left[\frac{F\psi_0}{2RT}\right] \quad (8)$$

Solution of eqs 7 and 8 provides the self-consistent surface charge density value. However, surface acid–base equilibria on other types of silica are characterized by two dissociation constants^{53,59} with corresponding $\text{p}K_{\text{a}}$ of 4.5 and 8.5. These values are associated with two different types of titratable silanol groups, present at the surface at 19% and 81% of the total number of ionized sites, respectively.^{53,59} The total surface charge density is therefore given through both contributions.

It follows that under ambient conditions ($\text{pH} \sim 7$) a small fraction of silanol groups are ionized, resulting in a negatively charged surface. The experimental

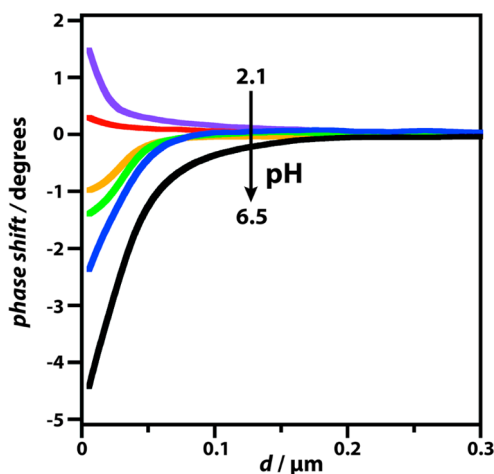


Figure 4. Experimental approach curves recorded with *ca.* 75 nm radius nanopipettes over a glass substrate at different solution pH (2.1, 2.5, 3.3, 3.7, 4.3, and 6.5 for purple, red, orange, green, blue, and black lines, respectively) performed with a bias, $\Delta V = -0.3$ V, applied to the nanopipette QRCE with respect to that in bulk solution. The arrow indicates an increase of the solution pH.

approaches of phase shift vs tip to surface distance, d , shown in Figure 4 for an applied bias $\Delta V = -0.3$ V to the nanopipette (and the DC data in Figure S6, Supporting Information SI-6) confirm the presence of a negative surface charge under these conditions, as surface-enhanced rectification induces a significant decrease of the AC phase value (and increase in the DC value, Figure S6, Supporting Information SI-6), when the nanopipette is brought into the vicinity of the substrate.

In more acidic solutions, increasing protonation of the silanol groups leads to an overall decrease of (absolute) surface charge density. Experimental phase shift-distance approach curves (Figure 4) under these conditions (pH = 2.1–4.3), reveal a smaller surface-enhanced rectification at lower pH. At pH values around 2.1–2.5, the AC phase shift-distance curves approach the behavior expected at an uncharged interface, in good agreement with a point of zero charge found on most of silica materials (typically, in the pH range 2–4).⁶⁰ Approach curves shown in Figure 4 evidence an almost linear variation of near-surface phase shift with pH over the range studied. On the basis of our simulations presented above (Figure 3c), this behavior suggests a linear-like titration of surface charges with pH. Dedicated modeling in the future could provide further insight into the protonation of this type of surface, although it needs to be recognized that other processes can complicate the analysis and interpretation. Although the electric field from the SICM probe is in the kilovolts per centimeter (kV cm^{-1}) range, a field of this magnitude is unlikely to induce changes in the local acid dissociation constants, as the Wein effect occurs at hundreds of kV cm^{-1} .^{61–63} However, local ion mobilities, particularly of protons at

surfaces,^{64,65} may be high and would need to be taken into account, with the tip-induced field possibly altering local pH values.

Surface Charge Mapping. Simultaneous mapping of surface charge distributions along with independent recording of surface topography is a particular advantage of the SICM technique described herein: an AC phase shift at 0 V mean bias can be used for a positionable feedback control, whereas measurements at $\Delta V \neq 0$ allow the detection of surface charge. We implemented this concept using a hopping voltammetric scan strategy, where the nanopipette was approached toward the substrate until a set value of a feedback parameter (phase shift, 0.5° used herein) was reached, followed by the recording of a cyclic voltammogram at that position (for which we present the linear part between -0.4 and 0.4 V) to sense the charge. The probe was then moved away from the surface and to the next pixel such that a spatial array of voltammograms was recorded. At each pixel, a voltammogram was recorded when the probe was away from the surface ($d = 500$ nm) and this response was subtracted from the surface voltammogram to reveal only the surface ICR. Examples of bias-dependent phase responses close to glass, polystyrene and in bulk are given in Supporting Information, section SI-7.

The capability of this approach was validated for a partial polystyrene film on a glass substrate, comprising heterogeneously distributed pinholes (exposing the glass) in the polystyrene layer. This substrate thus had both negatively charged glass regions, in 10 mM KCl solution, and neutral areas (uncharged polymer film). The topography recorded from the initial approaches to the substrate at $\Delta V = 0$ is shown in Figure 5a. This matches well to the typical topography recorded using AFM (Figure 5b). Taking into account the working distance (given by the set point value, corresponding to *ca.* 25 nm), SICM allows careful examination of substrate topography independently of surface charge. Even the smaller nanoscale pits in the film are apparent in the BM-SICM topography, an advance on our recent DM-SICM studies⁴⁴ in terms of resolution.

Significantly, the protocol used produces voltammetric data that can be represented as 81 image frames (phase and DC as a function of x, y position) at a set of different bias values at 10 mV intervals. Maps of the DC current at the surface, normalized by that in bulk, and AC phase shift at the surface with respect to bulk (subtracted) at -0.3 and 0.3 V are presented in Figure 5c–f. (A full image sequence is given in a form of video files nn5b02095_si_002.avi and nn5b02095_si_003.avi see Supporting Information, SI-8). These images, free from topographical effects, are highly revealing of the charge distribution across the surface, which is evidently very heterogeneous, from both the DC current and phase maps. In particular, it can be seen that there is an increase in the ion

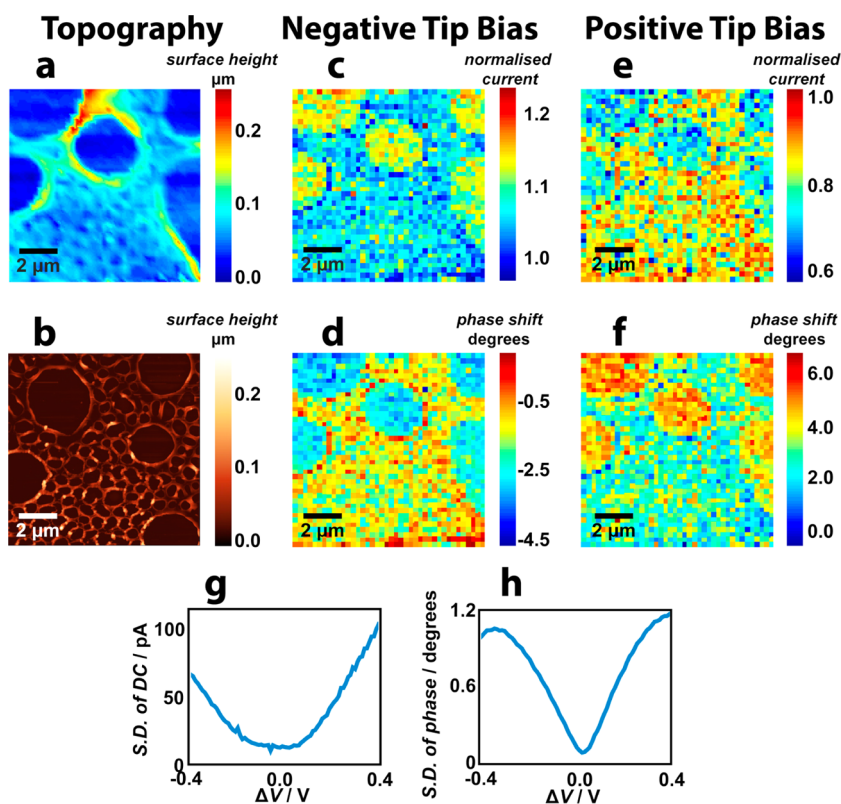


Figure 5. Simultaneous surface charge and topographical mapping over a nonuniform polystyrene film on glass. (a) Topography image recorded with a ~ 75 nm radius nanopipette operated in a hopping mode at 0 V bias offset and (b) an AFM image of a similar area of a substrate. (c–f) Example images of the normalized DC component and AC phase shift (with the response in bulk subtracted) of the ion current at -0.3 and $+0.3$ V mean bias values. Standard deviation of (g) ion currents and (h) bulk-corrected AC phase shift calculated across each image in a set of image frames acquired at 81 equally spaced bias values over the linear region scanned between -0.4 and $+0.4$ V.

current magnitude, when a higher conductance state is formed. That is, with a negative tip bias applied to the nanopipette over negatively charged regions (Figure 5c), where the normalized current magnitude ratio attains values between 1.1 and 1.2; or current diminution with positive tip bias in negatively charged regions where the normalized current attains values <0.8 (Figure 5e).

The corresponding phase behavior (Figure 5d,f) shows the interfacial charge effect with stronger contrast due to the fact that any change in the resistance is detected as a change in the ratio between the capacitive and resistive behavior of the nanopipette (and better signal-to-noise due to measurement with the lock-in amplifier). When the nanopipette experiences a low conductance state, the capacitance provides a larger contribution, which ideally has 90° phase shift with respect to the driving voltage, while at a high conductance state, a nanopipette acts more like as a resistor (0° phase shift for resistor circuit component).

The change of the conductance state of the nanopipette is also seen in voltammograms recorded at each pixel during imaging. As follows from the image sequences (see Supporting Information Figure S7 and the video files in section SI-8), the AC phase shift flips from negative to positive as the bias (ΔV) is scanned

from negative to positive values through 0 V. With the bias *ca.* 0 V, however, the phase signal across both the glass and polystyrene regions of the sample is close to the set point value because of the insensitivity of the phase to surface charge when $\Delta V = 0$, a key feature of this technique that we have described.

These data allow the standard deviation of every pixel value of each DC and phase image in the sequence to be calculated, with results shown in Figure 5g,h. It is clear that around $\Delta V = 0$, the images are relatively featureless (small standard deviation), but increase with a higher magnitude of applied potential, consistent with the greater contrast between the heterogeneously charged regions seen at ± 0.3 V. Interestingly, the region where the standard deviation attains a minimum is relatively broad (-0.2 to 0.1 V) for the DC signal, highlighting the lower sensitivity of the DC signal (Figure 5g) toward surface charge compared to the AC phase signal (Figure 5h), where the minimum of the standard deviation vs potential plot is much sharper.

CONCLUSIONS

This work provides a robust framework for nanoscale mapping of surface charge variations at substrates through sensing the ionic atmosphere of the diffuse

double layers formed at interfaces with a simple nanopipette approach. We have explored the versatility of BM-SICM for independent and accurate characterization of the topographical and charge properties of surfaces, using the capability of BM-SICM for performing experiments in the absence of a mean applied bias. In this situation, the nanopipette can be carefully positioned over the sample at a desired distance, using a set point value of the AC phase shift of the ionic current, which is shown to be a distance-dependent quantity, essentially unaffected by surface charge that makes it ideal for topographical mapping.

At nonzero net bias, however, BM-SICM becomes an extremely sensitive tool for probing surface charge *via* surface-induced rectification. Our experimental findings, supported by finite element simulations, suggest that AC components of the ionic current and, in particular, the phase shift are very responsive to the local resistance and, correspondingly, variations in

surface charge. The possibility of imaging heterogeneities of surface charge makes this technique indispensable for surface science, to unravel structure–functional relationships and to provide insights on interfacial processes and adsorption equilibria that modify the charge. Here, we have been able to resolve topography, free from surface-charge effects, and obtain semiquantitative insights into surface charge. Further quantitative analysis will require extremely detailed characterization of tip geometry and charge (which is often not the precise conical shape assumed in this and other work), and the charge/ICR characteristics of the nanopipette itself, as well as considerations of changes in ion mobility near surfaces. For future studies, transmission electron microscopy of glass nanopipettes⁶⁶ should allow better understanding of the probe geometry, and in perspective, this nanopipette approach should offer detailed quantification of surface charges.

MATERIALS AND METHODS

Solutions. Milli-Q reagent grade water (resistivity *ca.* 18.2 M Ω cm at 25 °C) was used for all solutions. For the BM-SICM approach curve measurements to glass, impedance studies and BM-SICM imaging, 10 mM KCl (Sigma-Aldrich, pH 6.5) solutions were prepared. To produce the polystyrene–glass substrate for imaging, polystyrene (Sigma-Aldrich) was dissolved in chloroform (Fisher Scientific) giving a solution (0.66 mg/mL) into which a glass slide was dip-coated (30 s) to create a polystyrene film. A solution of 3-aminopropyl triethoxysilane (APTES, Sigma-Aldrich) in toluene (2 μ L/mL) was used for glass surface modification for some experiments (dip-coated for 5 min). All impedance measurements and approach curve studies carried out on APTES samples were done in a slightly acidic solution of HCl (pH 3.4, Fisher Scientific) and KCl (9 mM). Solutions with varying ratios of KCl to HCl (keeping 10 mM constant ionic strength) were used to explore the effect of pH on the surface charge of glass. Approach curve measurements were also carried out toward glass in 1–100 mM KCl solutions to test the limits at which surface charge effects could be observed.

Nanopipettes. Nanopipettes (\sim 75 nm radius, inner taper angle 2.5–3.5°, dimensions measured with a Zeiss Supra55VP field emission scanning electron microscope) were pulled from borosilicate glass capillaries (o.d. 1.2 mm, i.d. 0.69 mm, Harvard Apparatus) using a laser puller (P-2000, Sutter Instruments; pulling parameters: Line 1: Heat 330, Fil 3, Vel 30, Del 220, Pul -, Line 2: Heat 330, Fil 3, Vel 40, Del 180, Pul 120). We deliberately chose to use a relatively large tip to produce a well-defined probe that was easily characterized. Although surface charge effects would be expected to be less prominent than on smaller tips,^{42,44} they are still shown to be significant with major implications for nanoscale SICM imaging as we discuss herein.

Substrates. Glass bottomed Petri dishes with detachable coverslips (3512, WillcoWells) were used as glass samples, either as received, after sonication in acetone (10 min), sonication in water (10 min) and plasma ashing in oxygen (1 min, 100 W), or after functionalization with either polystyrene or APTES. The polystyrene samples were dip coated to produce a heterogeneous thin neutral polystyrene film with exposed negatively charged glass regions, under the condition of the measurements (aerated, unbuffered, 10 mM KCl, pH 6.5).

Instrumentation. The basic instrumentation has been described elsewhere.^{45,67} Briefly, movement of the SICM probe in the direction normal to the substrate was controlled using a

piezoelectric positioning stage of range 38 μ m (P-753-3CD, Physik Instrumente) with lateral movement of the substrate controlled using a two-axis piezoelectric positioning system with a range of 300 μ m (Nano-BioS300, Mad City Labs, Inc.) The current-to-voltage converter used to measure currents was custom built. A lock-in amplifier (SR830, Stanford Research Systems) was used to generate the oscillating signal for BM-SICM approaches and to extract the phase and amplitude of the AC ion current. Data recording, as well as the probe position and voltage output control, was performed using a custom written LabVIEW (2013, National Instruments) program through an FPGA card (7852R, National Instruments). Impedance measurements were carried out using a Gamry Femtostat (FAS2-38039), with spectra acquired using Gamry Framework Data Acquisition Software (6.04).

Bias Modulated-Scanning Ion Conductance Microscopy Approaches. An oscillating bias (10 mV rms amplitude, 270 Hz) was applied between the two QRCEs about mean biases of -0.3 , 0 , and 0.3 V. All potentials quoted herein refer to the potential of the QRCE inside of the nanopipette with respect to the bulk QRCE. Nanopipettes were approached toward glass and APTES-coated substrates at 10 nm s⁻¹, and the DC, AC phase, and AC amplitude of the ionic current were recorded simultaneously. Approaches toward glass were also carried out in 10 mM electrolyte concentration with the pH varying between 2.1 (10 mM HCl) and 6.5 (10 mM KCl) to vary the surface charge on the glass substrate.

Bias Modulated-Scanning Ion Conductance Microscopy Imaging. BM-SICM images were acquired with a positionable nanopipette in a hopping mode, while applying a small oscillation to the bias (10 mV rms amplitude, 270 Hz) about 0 V. In this mode, the probe was translated toward the surface at each image pixel at 700 nm s⁻¹ until the surface was detected through a 0.5° increase in the AC phase signal. The piezo height at this point was used to generate topographical maps (as under these conditions the SICM response was relatively insensitive to surface charge effects; *vide infra*). The bias between the QRCEs was then swept linearly down to -0.4 V, reversed to 0.4 V, and finally returned to 0 V at a rate of 1 V s⁻¹, and the AC phase and DC were recorded, enabling polarity-dependent surface charge mapping. As well as movies of SICM response vs applied potential (presented over the range -0.4 to 0.4 V), representative maps at specific potentials as an average of several maps over potentials within ± 5 mV of the stated bias value were extracted, by taking average values of the AC and DC response for each pixel in the map.

FEM Simulations. A two-dimensional axisymmetric finite element method (FEM) model was constructed to mimic a nanopipette in bulk and in the vicinity of a charged surface (with a varying tip-to-substrate separation distance). Simulations were constructed in Comsol Multiphysics (version 4.4), using the transport of diluted species and electrostatics modules, using harmonic bias perturbation boundary conditions to simulate the AC behavior of the BM-SICM setup (for more details see Supporting Information SI-1).

Impedance Measurements. The Gamry Femtostat was connected between the two QRCEs: one in the nanopipette and one in bulk solution. Impedance spectra were collected at a set of frequencies between 1 Hz and 100 kHz, with 9 points per decade. Impedance measurements were performed with a 10 mV rms oscillation with 0 V mean bias.

Atomic Force Microscopy. Contact mode atomic force microscopy (AFM) (Catalyst, Bruker-Nano), using silicon tips on a nitride lever (SNL-10, Veeco), was employed for the analysis of sample substrates.

Conflict of Interest: The authors declare no competing financial interest.

Acknowledgment. This work was supported by the European Research Council through Project ERC-2009 AdG 247143-QUANTIF, EPSRC (Grant Number EP/F500378/1 through the MOAC DTC) and a Marie Curie IntraEuropean Fellowship 626158 FUSICIS (D.M.). The authors thank A. Colburn for the custom built electronics and K. McKelvey for the development of instrumentation and software.

Supporting Information Available: The SI includes FEM model details and schematic, impedance measurements. Also provided are typical AC amplitude approach curves and approach curves in electrolytes of high ionic strength. Theoretical DC approach curves and DC approach curves in varying pH are included, as well as experimental phase–voltage curves and the image sequences in the form of video files. The Supporting Information is available free of charge on the ACS Publications website at DOI: 10.1021/acsnano.5b02095.

REFERENCES AND NOTES

- Sahn, Ö.; Nusret Bulutcu, A. Effect of Surface Charge Distribution on the Crystal Growth of Sodium Perborate Tetrahydrate. *J. Cryst. Growth* **2002**, *241*, 471–480.
- Lin, N. H.; Shih, W.-Y.; Lyster, E.; Cohen, Y. Crystallization of Calcium Sulfate on Polymeric Surfaces. *J. Colloid Interface Sci.* **2011**, *356*, 790–797.
- Bodhak, S.; Bose, S.; Bandyopadhyay, A. Role of Surface Charge and Wettability on Early Stage Mineralization and Bone Cell–Materials Interactions of Polarized Hydroxyapatite. *Acta Biomater.* **2009**, *5*, 2178–2188.
- Hirsch, V.; Kinnear, C.; Moniatte, M.; Rothen-Rutishauser, B.; Clift, M. J. D.; Fink, A. Surface Charge of Polymer Coated Spions Influences the Serum Protein Adsorption, Colloidal Stability and Subsequent Cell Interaction. *Nanoscale* **2013**, *5*, 3723–3732.
- Chan, D. Y.; Pashley, R. M.; White, L. R. A Simple Algorithm for the Calculation of the Electrostatic Repulsion between Identical Charged Surfaces in Electrolyte. *J. Colloid Interface Sci.* **1980**, *77*, 283–285.
- Ohshima, H.; Healy, T. W.; White, L. R. Accurate Analytic Expressions for the Surface Charge Density/Surface Potential Relationship and Double-Layer Potential Distribution for a Spherical Colloidal Particle. *J. Colloid Interface Sci.* **1982**, *90*, 17–26.
- Tufenkji, N.; Elimelech, M. Breakdown of Colloid Filtration Theory: Role of the Secondary Energy Minimum and Surface Charge Heterogeneities. *Langmuir* **2005**, *21*, 841–852.
- Cuesta, A. Measurement of the Surface Charge Density of Co-Saturated Pt (111) Electrodes as a Function of Potential: The Potential of Zero Charge of Pt (111). *Surf. Sci.* **2004**, *572*, 11–22.
- Manzini, M. C.; Perez, K. R.; Riske, K. A.; Bozelli, J. C., Jr; Santos, T. L.; da Silva, M. A.; Saraiva, G. K. V.; Politi, M. J.; Valente, A. P.; Almeida, F. C. L.; et al. Peptide:Lipid Ratio and Membrane Surface Charge Determine the Mechanism of Action of the Antimicrobial Peptide Bp100. Conformational and Functional Studies. *Biochim. Biophys. Acta, Biomembr.* **2014**, *1838*, 1985–1999.
- Chen, L.; Mccrate, J. M.; Lee, J. C.; Li, H. The Role of Surface Charge on the Uptake and Biocompatibility of Hydroxyapatite Nanoparticles with Osteoblast Cells. *Nanotechnology* **2011**, *22*, 105708.
- Chung, T.-H.; Wu, S.-H.; Yao, M.; Lu, C.-W.; Lin, Y.-S.; Hung, Y.; Mou, C.-Y.; Chen, Y.-C.; Huang, D.-M. The Effect of Surface Charge on the Uptake and Biological Function of Mesoporous Silica Nanoparticles in 3T3-L1 Cells and Human Mesenchymal Stem Cells. *Biomaterials* **2007**, *28*, 2959–2966.
- Xiao, K.; Li, Y.; Luo, J.; Lee, J. S.; Xiao, W.; Gonik, A. M.; Agarwal, R. G.; Lam, K. S. The Effect of Surface Charge on *in Vivo* Biodistribution of Peg-Oligocholic Acid Based Micellar Nanoparticles. *Biomaterials* **2011**, *32*, 3435–3446.
- Dobrovolskaia, M. A.; Patri, A. K.; Simak, J.; Hall, J. B.; Semberova, J.; De Paoli Lacerda, S. H.; McNeil, S. E. Nanoparticle Size and Surface Charge Determine Effects of Pamam Dendrimers on Human Platelets *in Vitro*. *Mol. Pharmaceutics* **2011**, *9*, 382–393.
- Asati, A.; Santra, S.; Kaittanis, C.; Perez, J. M. Surface-Charge-Dependent Cell Localization and Cytotoxicity of Cerium Oxide Nanoparticles. *ACS Nano* **2010**, *4*, 5321–5331.
- Ghosh, P. S.; Kim, C.-K.; Han, G.; Forbes, N. S.; Rotello, V. M. Efficient Gene Delivery Vectors by Tuning the Surface Charge Density of Amino Acid-Functionalized Gold Nanoparticles. *ACS Nano* **2008**, *2*, 2213–2218.
- Bakhti, M.; Snaidero, N.; Schneider, D.; Aggarwal, S.; Möbius, W.; Janshoff, A.; Eckhardt, M.; Nave, K.-A.; Simons, M. Loss of Electrostatic Cell-Surface Repulsion Mediates Myelin Membrane Adhesion and Compaction in the Central Nervous System. *Proc. Natl. Acad. Sci. U. S. A.* **2013**, *110*, 3143–3148.
- Arjmandi, N.; Van Roy, W.; Lagae, L.; Borghs, G. Measuring the Electric Charge and Zeta Potential of Nanometer-Sized Objects Using Pyramidal-Shaped Nanopores. *Anal. Chem.* **2012**, *84*, 8490–8496.
- Sprycha, R. Electrical Double Layer at Alumina/Electrolyte Interface: I. Surface Charge and Zeta Potential. *J. Colloid Interface Sci.* **1989**, *127*, 1–11.
- Szekeres, M.; Tombác, E. Surface Charge Characterization of Metal Oxides by Potentiometric Acid–Base Titration, Revisited Theory and Experiment. *Colloids Surf., A* **2012**, *414*, 302–313.
- Gibson, G. T. T.; Mohamed, M. F.; Neverov, A. A.; Brown, R. S. Potentiometric Titration of Metal Ions in Ethanol. *Inorg. Chem.* **2006**, *45*, 7891–7902.
- Sánchez, J.; del Valle, M. Determination of Anionic Surfactants Employing Potentiometric Sensors—a Review. *Crit. Rev. Anal. Chem.* **2005**, *35*, 15–29.
- Heinz, W. F.; Hoh, J. H. Relative Surface Charge Density Mapping with the Atomic Force Microscope. *Biophys. J.* **1999**, *76*, 528–538.
- Miyatani, T.; Okamoto, S.; Rosa, A.; Marti, O.; Fujihira, M. Surface Charge Mapping of Solid Surfaces in Water by Pulsed-Force-Mode Atomic Force Microscopy. *Appl. Phys. A: Mater. Sci. Process.* **1998**, *66*, S349–S352.
- Miyatani, T.; Horii, M.; Rosa, A.; Fujihira, M.; Marti, O. Mapping of Electrical Double-Layer Force between Tip and Sample Surfaces in Water with Pulsed-Force-Mode Atomic Force Microscopy. *Appl. Phys. Lett.* **1997**, *71*, 2632–2634.
- Hillier, A. C.; Kim, S.; Bard, A. J. Measurement of Double-Layer Forces at the Electrode/Electrolyte Interface Using the Atomic Force Microscope: Potential and Anion Dependent Interactions. *J. Phys. Chem.* **1996**, *100*, 18808–18817.
- Manne, S.; Cleveland, J.; Gaub, H.; Stucky, G.; Hansma, P. Direct Visualization of Surfactant Hemimicelles by Force Microscopy of the Electrical Double Layer. *Langmuir* **1994**, *10*, 4409–4413.

27. Chen, C. C.; Zhou, Y.; Baker, L. A. Scanning Ion Conductance Microscopy. *Annu. Rev. Anal. Chem.* **2012**, *5*, 207–28.
28. Happel, P.; Thatenhorst, D.; Dietzel, I. D. Scanning Ion Conductance Microscopy for Studying Biological Samples. *Sensors* **2012**, *12*, 14983.
29. Rheinlaender, J.; Geisse, N. A.; Proksch, R.; Schäffer, T. E. Comparison of Scanning Ion Conductance Microscopy with Atomic Force Microscopy for Cell Imaging. *Langmuir* **2011**, *27*, 697–704.
30. Shevchuk, A. I.; Gorelik, J.; Harding, S. E.; Lab, M. J.; Klenerman, D.; Korchev, Y. E. Simultaneous Measurement of Ca²⁺ and Cellular Dynamics: Combined Scanning Ion Conductance and Optical Microscopy to Study Contracting Cardiac Myocytes. *Biophys. J.* **2001**, *81*, 1759–1764.
31. Hansma, P.; Drake, B.; Marti, O.; Gould, S.; Prater, C. The Scanning Ion-Conductance Microscope. *Science* **1989**, *243*, 641–643.
32. Novak, P.; Li, C.; Shevchuk, A. I.; Stepanyan, R.; Caldwell, M.; Hughes, S.; Smart, T. G.; Gorelik, J.; Ostanin, V. P.; Lab, M. J. Nanoscale Live-Cell Imaging Using Hopping Probe Ion Conductance Microscopy. *Nat. Methods* **2009**, *6*, 279–281.
33. Korchev, Y.; Milovanovic, M.; Bashford, C.; Bennett, D.; Sviderskaya, E.; Vodyanoy, I.; Lab, M. Specialized Scanning Ion-Conductance Microscope for Imaging of Living Cells. *J. Microsc.* **1997**, *188*, 17–23.
34. Ushiki, T.; Nakajima, M.; Choi, M.; Cho, S.-J.; Iwata, F. Scanning Ion Conductance Microscopy for Imaging Biological Samples in Liquid: A Comparative Study with Atomic Force Microscopy and Scanning Electron Microscopy. *Micron* **2012**, *43*, 1390–1398.
35. Yang, X.; Liu, X.; Zhang, X.; Lu, H.; Zhang, J.; Zhang, Y. Investigation of Morphological and Functional Changes During Neuronal Differentiation of Pc12 Cells by Combined Hopping Probe Ion Conductance Microscopy and Patch-Clamp Technique. *Ultramicroscopy* **2011**, *111*, 1417–1422.
36. Takahashi, Y.; Murakami, Y.; Nagamine, K.; Shiku, H.; Aoyagi, S.; Yasukawa, T.; Kanzaki, M.; Matsue, T. Topographic Imaging of Convuluted Surface of Live Cells by Scanning Ion Conductance Microscopy in a Standing Approach Mode. *Phys. Chem. Chem. Phys.* **2010**, *12*, 10012–10017.
37. Klenerman, D.; Korchev, Y. E.; Davis, S. J. Imaging and Characterisation of the Surface of Live Cells. *Curr. Opin. Chem. Biol.* **2011**, *15*, 696–703.
38. Bard, A. J.; Faulkner, L. R. *Electrochemical Methods: Fundamentals and Applications*; Wiley: New York, 1980; ch. 2.
39. Wei, C.; Bard, A. J.; Feldberg, S. W. Current Rectification at Quartz Nanopipet Electrodes. *Anal. Chem.* **1997**, *69*, 4627–4633.
40. Momotenko, D.; Cortes-Salazar, F.; Jossierand, J.; Liu, S.; Shao, Y.; Girault, H. H. Ion Current Rectification and Rectification Inversion in Conical Nanopores: A Perm-Selective View. *Phys. Chem. Chem. Phys.* **2011**, *13*, 5430–5440.
41. White, H. S.; Bund, A. Ion Current Rectification at Nanopores in Glass Membranes. *Langmuir* **2008**, *24*, 2212–2218.
42. Sa, N.; Lan, W.-J.; Shi, W.; Baker, L. A. Rectification of Ion Current in Nanopipettes by External Substrates. *ACS Nano* **2013**, *7*, 11272–11282.
43. Clarke, R. W.; Zhukov, A.; Richards, O.; Johnson, N.; Ostanin, V.; Klenerman, D. Pipette-Surface Interaction: Current Enhancement and Intrinsic Force. *J. Am. Chem. Soc.* **2013**, *135*, 322–9.
44. McKelvey, K.; Kinnear, S. L.; Perry, D.; Momotenko, D.; Unwin, P. R. Surface Charge Mapping with a Nanopipette. *J. Am. Chem. Soc.* **2014**, *136*, 13735–44.
45. McKelvey, K.; Perry, D.; Byers, J. C.; Colburn, A. W.; Unwin, P. R. Bias Modulated Scanning Ion Conductance Microscopy. *Anal. Chem.* **2014**, *86*, 3639–46.
46. Sa, N.; Baker, L. A. Rectification of Nanopores at Surfaces. *J. Am. Chem. Soc.* **2011**, *133*, 10398–10401.
47. Siwy, Z.; Heins, E.; Harrell, C. C.; Kohli, P.; Martin, C. R. Conical-Nanotube Ion-Current Rectifiers: The Role of Surface Charge. *J. Am. Chem. Soc.* **2004**, *126*, 10850–10851.
48. Shevchuk, A. I.; Frolenkov, G. I.; Sánchez, D.; James, P. S.; Freedman, N.; Lab, M. J.; Jones, R.; Klenerman, D.; Korchev, Y. E. Imaging Proteins in Membranes of Living Cells by High-Resolution Scanning Ion Conductance Microscopy. *Angew. Chem.* **2006**, *118*, 2270–2274.
49. Feng, J.; Liu, J.; Wu, B.; Wang, G. Impedance Characteristics of Amine Modified Single Glass Nanopores. *Anal. Chem.* **2010**, *82*, 4520–4528.
50. Sa, N.; Baker, L. A. Experiment and Simulation of Ion Transport through Nanopipettes of Well-Defined Conical Geometry. *J. Electrochem. Soc.* **2013**, *160*, H376–H381.
51. Kubeil, C.; Bund, A. The Role of Nanopore Geometry for the Rectification of Ionic Currents. *J. Phys. Chem. C* **2011**, *115*, 7866–7873.
52. Behrens, S. H.; Grier, D. G. The Charge of Glass and Silica Surfaces. *J. Chem. Phys.* **2001**, *115*, 6716–6721.
53. Fisk, J. D.; Batten, R.; Jones, G.; O'Reill, J. P.; Shaw, A. M. pH Dependence of the Crystal Violet Adsorption Isotherm at the Silica-Water Interface. *J. Phys. Chem. B* **2005**, *109*, 14475–14480.
54. Sabia, R.; Ukrainczyk, L. Surface Chemistry of SiO₂ and TiO₂-SiO₂ Glasses as Determined by Titration of Soot Particles. *J. Non-Cryst. Solids* **2000**, *277*, 1–9.
55. Zhuravlev, L. Concentration of Hydroxyl Groups on the Surface of Amorphous Silicas. *Langmuir* **1987**, *3*, 316–318.
56. Weber, A. E.; Baker, L. A. Experimental Studies of Resolution in Scanning Ion Conductance Microscopy. *J. Electrochem. Soc.* **2014**, *161*, H924–H929.
57. Edwards, M. A.; Williams, C. G.; Whitworth, A. L.; Unwin, P. R. Scanning Ion Conductance Microscopy: A Model for Experimentally Realistic Conditions and Image Interpretation. *Anal. Chem.* **2009**, *81*, 4482–4492.
58. Stumm, W.; Morgan, J. J. *Aquatic Chemistry: Chemical Equilibria and Rates in Natural Waters*; John Wiley & Sons: New York, 2012; Vol. 126.
59. Powell, H. V.; Schnippering, M.; Mazurenka, M.; Macpherson, J. V.; Mackenzie, S. R.; Unwin, P. R. Evanescent Wave Cavity Ring-Down Spectroscopy as a Probe of Interfacial Adsorption: Interaction of Tris (2, 2'-Bipyridine) Ruthenium (II) with Silica Surfaces and Polyelectrolyte Films. *Langmuir* **2009**, *25*, 248–255.
60. Papierer, E. *Adsorption on Silica Surfaces*; CRC Press: New York, 2000.
61. Eckstrom, H. C.; Schmelzer, C. The Wien Effect: Deviations of Electrolytic Solutions from Ohm's Law under High Field Strengths. *Chem. Rev.* **1939**, *24*, 367–414.
62. Onsager, L.; Kim, S. K. Wien Effect in Simple Strong Electrolytes. *J. Phys. Chem.* **1957**, *61*, 198–215.
63. Onsager, L. Deviations from Ohm's Law in Weak Electrolytes. *J. Chem. Phys.* **1934**, *2*, 599–615.
64. Slevin, C. J.; Unwin, P. R. Lateral Proton Diffusion Rates Along Stearic Acid Monolayers. *J. Am. Chem. Soc.* **2000**, *122*, 2597–2602.
65. Lockwood, G. K.; Garofalini, S. H. Proton Dynamics at the Water-Silica Interface Via Dissociative Molecular Dynamics. *J. Phys. Chem. C* **2014**, *118*, 29750–29759.
66. Zhou, L.; Zhou, Y.; Baker, L. A. Measuring Ions with Scanning Ion Conductance Microscopy. *Electrochem. Soc. Interface* **2014**, *47*.
67. Nadappuram, B. P.; McKelvey, K.; Al Botros, R.; Colburn, A. W.; Unwin, P. R. Fabrication and Characterization of Dual Function Nanoscale pH-Scanning Ion Conductance Microscopy (SICM) Probes for High Resolution pH Mapping. *Anal. Chem.* **2013**, *85*, 8070–8074.